

NIR Quantum Cutting in Y_2O_3 codoped with Ho^{3+} , Yb^{3+} phosphor synthesized by Solution Route

Seetu Jain¹, Puspallata¹, Prachi Tadge¹ and Sudeshna Ray^{1*}

¹Department of Physical Science, Rabindranath Tagore University, Bhopal, M.P. India

Abstract

An efficient route “Near-Infrared Quantum Cutting” and have been demonstrated in Ho^{3+} and Yb^{3+} co-activated Y_2O_3 sample, synthesized by a solution method. Quantum Cutting emission excited with 362 nm and 449 nm, of (1%) Ho^{3+} and (5 %) Yb^{3+} codoped Y_2O_3 samples, reveals the efficient emission in the green region which corresponds to $^5S_2 - ^5I_8$ transition of Ho^{3+} at 549 nm in visible region. Ho^{3+}/Yb^{3+} co-doped yttrium oxide phosphors have been synthesized and the phase analysis by powder XRD, measurement of SEM images, Steady State and Time-Resolved Photoluminescence Study has been investigated in detail. An orthorhombic of Y_2O_3 : Ho^{3+} , Yb^{3+} phosphor show a pure phase by X-Ray diffraction and Photoluminescence emission (PL) spectra, reveals the efficient emission in the green region which corresponds to $^5S_2 - ^5I_8$ transition of Ho^{3+} . This type of NIR QC phosphors has great promises in energy conversion for c-Si solar cell applications.

1. Introduction:

Global energy consumption is on the rise and sustainable energy production based on the direct conversion of the energy radiated from the sun into electricity, has achieved significant importance for the generation of sufficient energy to meet the long-term worldwide energy demand [1, 2]. Harnessing solar energy through photovoltaic (PV) technology constitutes a promising route for the generation of green and renewable energy. One of the major factors limiting the efficiency of solar cells is the ‘spectral mismatch’ between the energy distribution of photons in the incident solar spectrum and the band-gap of a semiconductor material used in Solar Cell. In the ‘Smart Photon Management’ of the Solar Spectrum, spectral modification by converting sub-band-gap photons to supra-band-gap photons, is one of the third generation concept which has been suggested to overcome the classical efficiency limit of photovoltaic devices [3-5]. All photovoltaic devices exhibit a certain absorption threshold, and incident photons with energy below this threshold do not contribute to current generation in solar cell. On the other hand, photons with energy larger than the band-gap of the semiconductor constituting the solar cell are absorbed but the excess energy is lost due to thermalization of the generated electrons. The strategy, termed as third generation solar photon conversion involves the incorporation of a passive luminescence layer consisting of down-conversion, down-shifting and upconversion phosphors, in PV cell [6].

However, despite the considerable development of the PV technologies over the past decades, the high production and fabrication cost of the materials coupled with limited power conversion efficiency have restricted the extensive use of this environment-friendly technology for power generation. On the other hand, quantum cutting (QC) or down-conversion luminescence materials yield two lower energy NIR photons by cutting a high energy UV photon, leading to quantum efficiency of more than 100%, is used for the spectral conversion of photons which are responsible for the generation of thermalization loss [16, 17].

Generally the power conversion efficiency (PCE) of DSSCs can be impacted by many factors such as light harvesting efficiency, electron injection efficiency and the rate of undesirable charge recombination [18]. Although, all the rare-earths except La^{3+} and Lu^{3+} , are well known for their sharp luminescence emissions originating from $4f-4f$ transition, very few rare earths such as Er^{3+} , Tm^{3+} , Ho^{3+} owing to their ladder-like energy levels, are suitable for upconversion emission. Furthermore, for the realization of all the three optical processes, i.e. for multimodal emission, couple of lanthanides either separately or co-doped with Yb^{3+} are suitable. Till date, very few papers have been published on rare-earth doped oxide phosphors exhibiting color emission tunability as well as exhibiting multimodal emissions.

In the present work, the down-conversion (DC), in $\text{Ho}^{3+}/\text{Yb}^{3+}$ codoped Y_2O_3 phosphors have been realized. Concentration optimized $\text{Y}_2\text{O}_3:\text{Ho}^{3+}/\text{Yb}^{3+}$ phosphor shows efficient energy transfer from Ho^{3+} to Yb^{3+} when excited by 449 nm.

2. Experimental

2.1 Syntheses of Phosphors

$\text{Y}_2\text{O}_3:\text{Ho}^{3+}(1\%),\text{Yb}^{3+}(5\%)$, phosphors samples have been prepared by “complex based precursor solution method” using triethanolamine (TEA) as complexing agent. For the synthesis of Ho^{3+} , Yb^{3+} doped Y_2O_3 , solid powder of Yttrium Nitrate [$\text{Y}(\text{NO}_3)_3$], Holmium Nitrate [$\text{Ho}(\text{NO}_3)_3$] and Ytterbium Nitrate [$\text{Yb}(\text{NO}_3)_3$] have been dissolved in double distilled water to make the stock solutions of Yttrium Nitrate, Holmium Nitrate and Ytterbium Nitrate, respectively. $\text{Y}(\text{NO}_3)_3$ and $\text{Ho}/\text{Yb}(\text{NO}_3)_3$ solutions are taken in different stoichiometric ratios in order to synthesize samples. When complete dehydration occurred, the nitrates themselves decomposed, with the evolution of brown fumes of nitrogen dioxide, leaving behind a voluminous, organic-based, black, fluffy powder, i.e., the precursor powder. The precursor mass was then calcined at 650 °C for 2 h and annealed at 1000 °C for 2 h to get the required samples.

3. Result and Discussion

3.1 Crystal Structure and Phase Purity analysis by X-ray Diffraction (XRD)

The phase purity of the synthesized samples has been checked by powder XRD. Figs. 1 present the XRD patterns of $\text{Y}_2\text{O}_3:\text{Ho}^{3+}(1\%), \text{Yb}^{3+}(5\%)$. From Fig. 1, the XRD pattern of the phosphor shows the positions and relative intensity of the diffraction peaks for the as-prepared samples which can be indexed to the $Ia-3$ (206) space group with the standard cards of cubic Y_2O_3 (JCPDS#88-1040), which do not show any change with a variation in Yb^{3+} concentration even up to 30 mol%. No impurity phase is observed in XRD patterns, demonstrating $\text{Ho}^{3+}/\text{Yb}^{3+}$ are all incorporated into Y_2O_3 and formed a solution structure. This confirms an effective doping of Ho^{3+} and Yb^{3+} ions on Y^{3+} site.

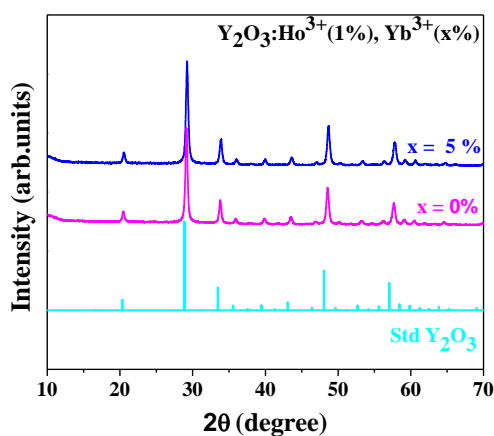


Fig. 1 XRD patterns of (a) $\text{Y}_2\text{O}_3:\text{Ho}^{3+}(1\%), \text{Yb}^{3+}(5\%)$; with the standard XRD data of cubic Y_2O_3 (JCPDS# 88-1040).

The morphology and the size of as-synthesized nanophosphors have been measured by Transmission Electron Microscopy (TEM). Figs. 2 display the TEM of $\text{Ho}^{3+}/\text{Yb}^{3+}$ -doped yttria nanoparticles annealed at 1000°C for 2 h. From Figs 2, it is evident that all nanoparticles exhibit spherical shape and the average size of the nanoparticles have been estimated by measuring over 50 particles and the average size of the nanoparticles have been found to be ~ 30 nm.

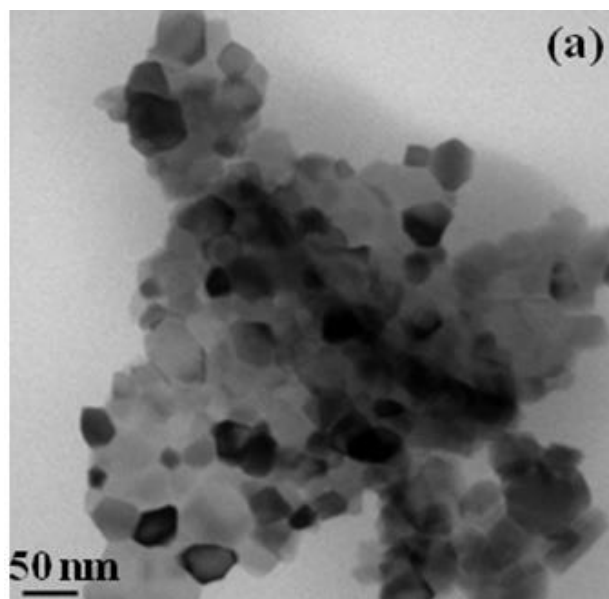
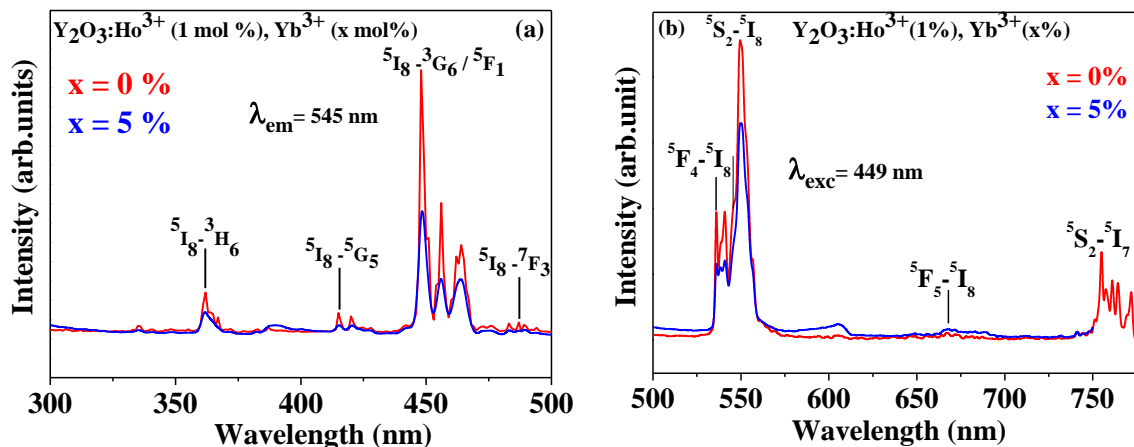


Fig. 2 TEM image of $\text{Y}_2\text{O}_3:\text{Ho}^{3+}(1\%), \text{Yb}^{3+}(5\%)$ phosphor

3.2 Luminescence Properties

Photoluminescence Excitation and Emission Spectra of $\text{Y}_2\text{O}_3:\text{Ho}^{3+}(1\%), \text{Yb}^{3+}(x\%)$ ($x = 0, 5, 10$ and 20) phosphors have been presented in Figs. 3(a) and (b). The host absorption band of Y_2O_3 lies in 200–300 nm regimes, accordingly the excitation spectra have been recorded in 300–500 nm regions only. Excitation Spectra is comprised of a large number of sharp absorption peaks located at 362 nm, 420 nm, 449 nm and 494 nm corresponding to $^5\text{I}_8 \rightarrow ^3\text{H}_6$, $^5\text{I}_8 \rightarrow ^5\text{G}_5$, $^5\text{I}_8 \rightarrow ^3\text{G}_6 / ^5\text{F}_1$ and $^5\text{I}_8 \rightarrow ^7\text{F}_3$ of Ho^{3+} respectively. To understand the energy transfer from Ho^{3+} to Yb^{3+} as well as the down-conversion mechanism, a schematic energy level diagram of $\text{Ho}^{3+} \rightarrow \text{Yb}^{3+}$ ions with radiative electronic transitions is shown in Fig.4 in supporting information. A variation in the intensity of the excitation peaks is observed with the enhancement of the Yb^{3+} concentration in codoped samples. It has been perceived that, the intensity of the excitation peaks decreases followed by the increase in the concentration of Yb^{3+} .

The visible emission spectra are measured by exciting the phosphors at 449 nm excitation wavelength, which is attributed to the absorption of $\text{Ho}^{3+}: ^5\text{I}_8 \rightarrow ^5\text{G}_6 / ^5\text{F}_1$ transition and is presented in Fig. 3(b). PL emission spectra exhibit two evident emission bands placed at 549 nm and 755 nm in the range of 500–800 nm corresponding to $^5\text{F}_4 / ^5\text{S}_2 \rightarrow ^5\text{I}_8$ and $^5\text{F}_4 / ^5\text{S}_2 \rightarrow ^5\text{I}_7$ transitions of the Ho^{3+} ion, respectively. Besides, there are two weak emission peaks at 536 nm and 667 nm, as presented in Fig. 3(b), which are attributed to $^5\text{F}_3 \rightarrow ^5\text{I}_8$ transition and $^5\text{F}_5 \rightarrow ^5\text{I}_8$ transition of Ho^{3+} ion, respectively. It is interesting to mention that Ho^{3+} ion in the ground state ($^5\text{I}_8$) is excited to $^5\text{G}_6 / ^5\text{F}_1$ state after excitation by 449 nm. Subsequently, $^5\text{F}_4 / ^5\text{S}_2$ level and $^5\text{F}_5$ level can be populated by non-radiative relaxation processes from the corresponding upper states. Here, non-radiative multiphonon relaxation process dominates over radiative decay, which owes to the small energy gap between the upper state and $^5\text{F}_4 / ^5\text{S}_2$ and $^5\text{F}_5$ levels.



4. Conclusion

Fig. 4 Excitation (a) and emission (b) Spectra of $\text{Ho}^{3+}/\text{Yb}^{3+}$ codoped Y_2O_3 phosphors with

$\text{Ho}^{3+}/\text{Yb}^{3+}$ varying codoped concentrations of Y_2O_3 phosphors have been synthesized and the cubic phase analysis by powder XRD, TEM images, and Photoluminescence Study has been investigated in detail. Structure of the proposed phosphor has been determined by XRD. A Photoluminescence emission (PL) spectra, reveals the efficient emission in the green region which corresponds to ${}^5\text{S}_2 - {}^5\text{I}_8$ transition of Ho^{3+} ion. This type of NIR QC phosphors has great promises in energy conversion for c-Si solar cell applications.

References

1. Scholes, G. D.; Fleming, G. R.; Olaya-Castro, A.; Grondelle, R.V.; Lessons from nature about solar light harvesting. *Nat. Chem.* **2011**, *3*, 763-774.
2. Lewis, N. S.; Toward Cost-Effective Solar Energy Use. *Science* **2007**, *315*, 798-801.
3. Van der ende, B. M.; Aarts, L.; Meijerink, A.; Lanthanide ions as spectral converters for solar cells. *Phys. Chem. Chem. Phys.* **2009**, *11*, 11081-11095.
4. Green, M. A.; Solar Cells: Operating Principles, Technology and Systems Application. Englewood Cliffs, NJ: Prentice-Hall, **1982**.
5. Luque, A.; Hegedus, S.; Eds. Handbook of Photovoltaic Science and Engineering. Wiley: Chichester, U. K, **2003**.
6. Martí, A.; Luque, A.; Next Generation Photovoltaics, High Efficiency through Full Spectrum Utilization, CRC Press Talor and Francis, ISBN No.1420033867, **2004**.
7. O'regan, B.; Gratzel, M.; Super-spiral structures in an excitable medium. *Nature*, **1991**, *353*, 737-740.

8. Gratzel, M.; Photo electrochemical cells. *Nature*, **2001**, *414*, 338.
9. Yang, H.; Peng, F.; Zhang, Q.; Liu, W.; Sun, D.; Zhao Y.; Wei, X.; Strong upconversion luminescence in LiYMo₂O₈: Er, Yb towards efficiency enhancement of dye-sensitized solar cells. *Opt. Mater.*, **2013**, *35*, 2338-2342.
10. Auzel, F.; Upconversion and anti-Stokes processes with f and d ions in solids. *Chem. Rev.* **2004**, *104*, 139-173
11. Haase, M.; Schafer, H.; Upconverting nanoparticles. *Angew. Chem. Int. Ed.* **2011**, *50*, 5808-5829.
12. Liu, X.; Yan, C.; Capobianco, J. A.; Photon upconversion nanomaterials. *Chem. Soc. Rev.* **2015**, *44*, 1299-1301.
13. Zhou, Bo.; Shi, B.; Jin, D.; Liu, X.; Controlling upconversion nanocrystals for emerging application. *Nat. Nanotech.* **2015** *10*, 924-936
14. Goldschmidt, J. C.; Fischer, S.; Upconversion for Photovoltaics – a Review of Materials, Devices and Concepts for Performance Enhancement. *Adv. Opt. Mater.* **2015**, *3*, 510-519.
15. Rudiger, M.; Fischer, S.; Frank, J.; Ivaturi, A.; Richards, B. S.; Kramer, K.W.; Hermle M.; Goldschmidt C.; Bifacial *n*-type silicon solar cells for upconversion applications. *Sol. Energy Mater. Sol. Cells* **2014**, *128*, 57-68.
16. Yu, D. C.; Rodriguez, R. M.; Zhang, Q. Y.; Meijerink, A.; Rabouw, F. T.; Multi-photon quantum cutting in Gd₂O₃:Tm³⁺ to enhance the photo-response of solar cells. *Light Sci. & Appl.* 2015, *4e344*, 1-8.
17. Zhang Q. Y.; Huang, X. Y.; Recent progress in quantum cutting phosphors. *Prog. in Mater. Scie.* **2010**, *55*, 353-427.
18. Ning, Z.; Fu, Y.; Tian, H.; Improvement of dye-sensitized solar cells: what we know and what we need to know. *Energy Environ. Sci.*, **2010**, *3*, 1170-1181.
19. Shan, G. B.; Demopoulos, G. P.; Near Infrared Sunlight Harvesting in Dye Sensitized Solar Cells Via the Insertion of an Upconverter TiO₂ Nanocomposite Layer. *Adv. Mater.* **2010**, *22* 4373-4377.
20. Liu, M.; Lu, Y.; Xie, Z. B.; Chow, G. M.; Enhancing near-infrared solar cell response using upconverting transparent ceramics *Sol. Energy Mater. & Sol. Cells*, **2011**, *95*, 800-803.
21. Shan, G. B.; Assaoudi, H.; Demopoulos G. P.; Enhanced Performance of Dye-Sensitized Solar Cells by Utilization of an External, Bifunctional Layer Consisting of Uniform β-NaYF₄:Er³⁺/Yb³⁺Nanoplatelets, *ACS Appl. Mater. Interface*, **2011**, *3*, 3239-3243.
22. Li, P.; Peng, Q.; Li, Y.; Dual Mode Luminescent Colloidal Spheres from Monodisperse Rare Earth Fluoride Nanocrystals. *Adv. Mater.*, **2009**, *21*, 1945-1948.

23. Ivanova, S.; Pelle, F.; Tkachuk, A.; Joubert, M. F.; Guyot Y.; Gapontzev, V. P.; Upconversion luminescence dynamics of Er-doped fluoride crystals for optical converters. *J. Lumin.* **2008**, *128*, 914-917.
24. Wang, G.; Peng Q.; Li, Y.; Upconversion Luminescence of Monodisperse $\text{CaF}_2:\text{Yb}^{3+}/\text{Er}^{3+}$ Nanocrystals. *J. Am. Chem. Soc.* **2009**, *131*, 14200-14201.
25. Zhang, F.; Wan, Y.; Yu, T. Zhang, F.; Shi, Y.; Xie, S.; Li, Y.; Xu, L.; Tu, B.; Zhao D.; Uniform nanostructured arrays of sodium rare-earth fluorides for highly efficient multicolor upconversion luminescence. *Angew. Chem. Int. Ed.* **2007**, *46*, 7976-7979.
26. Kramer, K.W.; Biner, D.; Frei, G.; Gudel, H. U.; Hehlen, M. P.; Luthi, S. R.; Hexagonal Sodium Yttrium Fluoride Based Green and Blue Emitting Upconversion Phosphors *Chem. Mater.* **2004**, *16*, 1244-1251.
27. Jin, X.; Li, H.; Li, D.; Zhang, Q.; li, F.; Sun, W.; Chen, Z.; Li Q.; Role of ytterbium-erbium co-doped gadolinium molybdate ($\text{Gd}_2(\text{MoO}_4)_3:\text{Yb}^{3+}/\text{Er}^{3+}$) nanophosphors in solar cells. *Opt. Express* **2016**, *24*, A1276-A1787.
28. Yang, H.; Peng, F.; Zhang, Q.; Liu, W.; Sun, D.; Zhao, Y.; Wei, X.; Strong upconversion luminescence in $\text{LiYMo}_2\text{O}_8:\text{Er}^{3+},\text{Yb}^{3+}$ towards efficiency enhancement of dye-sensitized solar cells. *Opt. Mater.* **2013**, *35*, 2338-2342.
29. Yim, D. K.; Cho, I.S.; Lee, S.; Kwak, C.; H.; Kim, D. H.; Lee, J. K.; Hong, K. S.; Synthesis and Characteristics of Tb-Doped Y_2SiO_5 Nanophosphors and Luminescent Layer for Enhanced Photovoltaic Cell Performance. *J. of Nanosci. & Nanotech.* **2011**, *11*, 8748-8753.
30. Du, P.; Lim, J. H.; Kim, S. H.; Yu, J. S.; Facile synthesis of $\text{Gd}_2\text{O}_3:\text{Ho}^{3+}/\text{Yb}^{3+}$ nanoparticles: an efficient upconverting material for enhanced photovoltaic performance of dye sensitized solar cells. *Opt. Mater. Express*, **2016**, *6*, 1898-1904.